Two-Dimensional Phase Transitions of Chemisorbed Uracil on Ag(111): Modeling of Short- and Long-Time Behavior

ARTICLE *in* THE JOURNAL OF PHYSICAL CHEMISTRY · NOVEMBER 1996

Impact Factor: 2.78 · DOI: 10.1021/jp961663z

3 AUTHORS, INCLUDING:

Rolando Guidelli
University of Florence
226 PUBLICATIONS **3,889** CITATIONS
SEE PROFILE

Maria Luisa Foresti
University of Florence
115 PUBLICATIONS **1,944** CITATIONS
SEE PROFILE

Two-Dimensional Phase Transitions of Chemisorbed Uracil on Ag(111): Modeling of Short- and Long-Time Behavior

Rolando Guidelli,* Maria Luisa Foresti, and Massimo Innocenti

Department of Chemistry, Florence University, Via G. Capponi 9, 50121 Florence, Italy

Received: June 5, 1996; In Final Form: August 9, 1996[⊗]

The short-time behavior of uracil two-dimensional phase transition on Ag(111) from aqueous 0.05 M $KClO_4$ at 25 °C was investigated at uracil concentrations ranging from 1×10^{-4} to 1×10^{-3} M by measuring the time dependence of the charge following potential steps from −1.5 V/SCE, where there is indirect evidence that uracil is completely desorbed, to potentials positive to −0.5 V/SCE, where uracil is chemisorbed, over a period of 0.6 s. The corresponding long-time behavior was followed on the basis of differential capacity vs time curves over a period of a few minutes. The short-time behavior is interpreted by a model that accounts for diffusion-controlled random adsorption of uracil molecules according to a Frumkin isotherm, followed by their progressive nucleation and by growth of the resulting clusters; the effect of nucleation with exponential decay of the nucleation rate and ingestion effects are also considered. The long-time behavior is explained by a model that considers the formation of a new two-dimensional phase and the nucleation and growth of water holes within this new phase, up to the attainment of a steady state.

Introduction

Two-dimensional (2D) phase transitions of electroinactive organic compounds at the mercury/water interface have been extensively investigated from both a thermodynamic and a kinetic point of view, and several models have been proposed for the interpretation of the experimenal behavior (for two recent reviews, see refs 1 and 2). Despite an early study of camphor adsorption on Zn(0001),[3] 2D phase transitions on solid electrodes and, more particularly, on single-crystal faces have received increasing attention only in recent years. The few systems so far investigated are pyridine on Au(100),[4] Au(111),[5] and Ag(210),[6] thymine on Cd(0001),[7] coumarin on Au(111) and Au(100)-(hex),[8] uridine on Au(111),[9,10] uracil on Au(111), Au(100)-(hex),[11] Ag(111), and Ag(100),[12] thymine on Ag(111) and Ag(100),[13] and cytosine on Au(111).[14] Ordered adlayer structures have also been reported for thymine, cytosine, guanine, and adenine on Au(111) employing in situ STM.[15]

From the electrochemical behavior of the structurally similar compounds uracil and thymine, some general trends emerge. Thus, uracil on Au(111), on the (111)-like densely packed surface of reconstructed Au(100)-(hex),[11] on Ag(111), and on Ag(100)[13] as well as thymine on Ag(111) and on Ag(100)[13] exhibit three well-defined adsorption states. When proceding toward more positive potentials they are as follows: a dilute, gaslike disordered state (state I); an ordered, liquid-like physisorbed state that shows the typical behavior of a 2D condensed film as is known from the mercury/water interface (state II); a further ordered, chemisorbed state that shows an extreme stability even at relatively high temperatures and is relatively insensitive toward the surface crystallographic orientation (state IV). A less defined state III, which probably corresponds to a reorientational transition, is identified between states II and IV. Even the structurally similar cytosine exhibits states I, III, and IV on Au(111), but lacks the physisorbed state II.[14] STM images of the chemisorbed adlayers of uracil[11] and of cytosine[14] on Au(111) have been reported.

Of the above organic compounds, uracil is the one that has been more extensively studied on mercury (ref 16 and references therein), especially by differential capacity measurements. The differential capacity C exhibits a "short-time" as well as a "long-time" behavior.[17,18] The short-time behavior is amenable to an intepretation based on the well-known Canac−Kolmogorov−Avrami−Evans equations[19−22] for 2D polynucleation and growth, or a generalized version[16] of these equations. The long-time behavior is characterized by an increase in capacity, which ultimately tends to a constant value.[17] A similar behavior had been previously observed by Pospísil with tris(2,2′-bipyridine) complexes of Co(II), Ni(II), and Fe(II).[23] Wandlowski and Pospísil first ascribed this phenomenon to multilayer growth.[17] Subsequently, however, the fractal character of the uracil films on mercury led these authors to favor an alternative explanation,[18] which Pospísil et al.[24] extended to the similar long-time adsorption behavior of difenzoquat. Briefly, the initial stage of film nucleation and growth is followed by nucleation and growth of water-filled holes inside large islands of the preformed condensed organic film. The increasing coverage of the electrode by the condensed organic film increases the probability of formation of water-filled holes, which may ultimately lead to a steady-state apparent limiting coverage.[24]

The potentiostatic current−time transients accompanying the polynucleation and growth (PG) of by far the majority of the organic compounds on single-crystal faces (and also the underpotential deposition of copper on Au(111)[25]) are characterized by an exponential decay, which precedes the typical rising section followed by the gradual decay toward zero current normally encountered in PG processes on mercury. To explain the initial exponential decay and the resulting minimum in the current−time transients, two parallel and entirely independent pathways have been postulated:[11,25] (i) random adsorption (RA) at microscopic surface inhomogeneities and rough patches that do not allow the formation of a two-dimensional, laterally organized compact film due to geometric and/or energetic limitations; (ii) PG on the structurally well ordered portion of the electrode surface. RA is regarded as responsible for the initial exponential decay, whereas PG is treated within the framework of the well-established Avrami model[21] normally adopted at mercury electrodes. Incidentally, according to a model for such a "noncompetitive" case characterized by

[⊗] Abstract published in *Advance ACS Abstracts,* November 1, 1996.

S0022-3654(96)01663-2 CCC: $12.00

structurally different surface areas,[26] linear potential sweep voltammograms are expected to exhibit two distinct peaks, except for the particular situation in which the RA and PG processes proceed at comparable rates.

Simultaneous RA and PG has been considered in a number of models that, while excluding incorporation of the randomly adsorbed molecules into islands of the condensed phase, account for different degrees of coupling between the RA and PG processes. Thus, Bosco and Rangarajan[27] account for the effect of the surface coverage S by the condensed phase on the rate $d\theta/dt$ of RA by writing

$$d\theta/dt = k_{ads}c(1 - \theta - S) - k_{des}\theta \quad (1)$$

where θ is the surface coverage by the randomly adsorbed molecules, c is the bulk surfactant concentration, and k_{ads}, k_{des} are the rate constants for adsorption and desorption, respectively. This is a unidirectional coupling, in that PG is not at all affected by RA, and leads to some inconsistencies, as pointed out by Noel et al.[26] These authors proposed to remove this unsatisfactory feature by introducing the multiplying factor $(1 - \theta)$ in the integral form of the Avrami equation:

$$S = (1 - \theta)[1 - \exp(-S_{ex})] \quad (2)$$

where S_{ex} is the "extended" area. Later on, Bhattacharjee and Rangarajan[28] recognized the inconsistency in Bosco and Rangarajan's model[27] and proposed a more satisfactory way to account for the effect of RA on PG by incorporating the same $(1 - \theta - S)$ multiplying factor of eq 1 into the differential form of the Avrami equation:

$$dS/dt = (1 - \theta - S)\, dS_{ex}/dt \quad (3)$$

All these models predict potentiostatic current−time transients with a descending branch, a subsequent rising section, and a final exponential decay toward zero.[27,28] Direct incorporation of randomly adsorbed molecules into growing clusters of the condensed phase was considered by de Levie et al.[29,30]

The present note describes the "short-time" behavior of uracil 2D phase transition on Ag(111) from aqueous 0.05 M $KClO_4$ on the basis of charge vs time transients, as well as the corresponding "long-time" behavior on the basis of differential capacity vs time curves. Our attention has been exclusively focused on the chemisorbed state (state IV in ref 12). Our measurements were carried out at 25 °C with uracil concentrations ranging from 1×10^{-4} to 1×10^{-3} M. Under these conditions the physisorbed state (state II in ref 12) does not form, since the minimum uracil concentration at which 2D condensation of the physisorbed state takes place is about equal to 1×10^{-2} M.[12] The short-time behavior will be interpreted on the basis of a model that accounts for the progressive incorporation of randomly adsorbed molecules into clusters of a condensed phase, whereas the long-time behavior will be explained by a model that considers the formation of a new condensed phase and the nucleation and growth of water holes within this new phase up to the attainment of a steady state.

Experimental Section

For the silver single-crystal electrode and cell arrangement the reader is referred to refs 31 and 32. All measurements were carried out at 25 ± 0.2 °C. Fluka analytical reagent grade 2,4-dihydroxypyrimidine (uracil) and Merck $KClO_4$ were recrystallized twice from bidistilled water and then dried. All sets of experimental measurements at different concentrations were carried out by adding increasing amounts of a deaerated 0.02 M stock solution of uracil to a previously deaerated aqueous solution of 0.05 M $KClO_4$ by means of a Hamilton syringe acted by a digital-display micrometer screw of 0.005 mm pitch. After each uracil addition, the electrode was lifted in order to keep the contact area with the solution constant. The proper position of the electrode was found by keeping constant the value of the compensation resistance used in the positive feedback adjustment. In fact, under the present conditions the electrolyte concentration is constant, and hence the value of the uncompensated resistance around the working electrode is exclusively determined by its area. All operations connected with positioning the electrode were facilitated by the use of a device activated by means of an oleopneumatic piston and connected to a digital position sensor.[32] To prevent a possible decrease in the solution level caused by the continuous bubbling into the cell, the argon used for the deaeration was previously bubbled into a vessel containing a solution of the same composition as that in the cell.

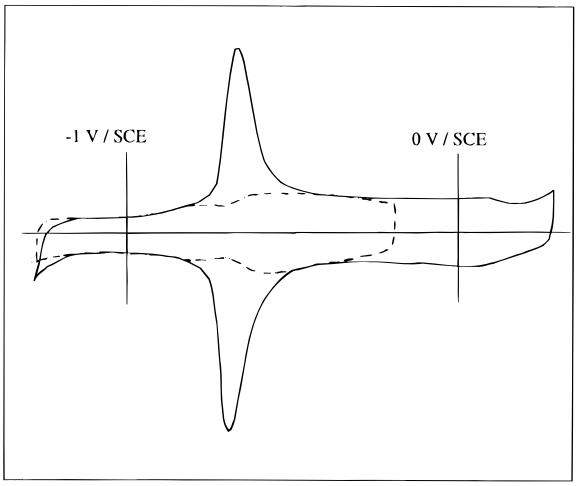

Figure 1. Cyclic voltammogram of 2×10^{-4} M uracil from aqueous 0.05 M $KClO_4$ on Ag(111) at 25 °C. The dashed curve was obtained in the absence of uracil.

Cyclic voltammetric and chronocoulometric measurements were carried out under the control of a Data General DG10 microcomputer: the voltage signal, modulated according to the technique employed, was generated by the microcomputer through digital-to-analog conversion and applied to the cell via an Amel Model 551 fast-rise potentiostat. In the cyclic voltammetric measurements the potential was scanned between two chosen values, and the current response from the cell was recorded by a 7090A HP plotting system. In differential capacity measurements the ac signal generated by a 1250 Solartron Frequency Response Analyzer was superimposed on the bias potential E applied by the microcomputer. An equivalent circuit consisting of a resistor and a capacitor in series was assumed in the calculation. The wholly computerized experimental apparatus permitted us to switch from one technique to another, via software, while constantly keeping the working electrode under a controlled applied potential.

Results

Figure 1 shows the cyclic voltammogram of 2×10^{-4} M uracil at 25 °C. The peak at ca. −0.7 V marks the transition from the more negative potential region, where uracil molecules are randomly adsorbed, to the more positive one, where the chemisorbed condensed phase is formed. Incidentally, at the higher uracil concentrations and lower temperatures adopted by Wandlowski[12] we also observed the two peaks reported by this author, which are indicative of both a physisorbed and a

chemisorbed condensed phase. It can be seen that the presence of uracil causes hydrogen discharge to occur at less negative potentials than in a solution of 0.05 M $NaClO_4$ alone. This catalytic effect is common to the majority of organic compounds, including alcohols,[31,32] and was also observed by Wandlowski with uracil on silver single-crystal electrodes (Th. Wandlowski, private communication; see also the incipient hydrogen discharge at about −1.2 V in Figure 1A of ref 12). That the cathodic current shown in Figure 1 at the most negative potentials is due to hydrogen evolution is indicated by the fact that by keeping the applied potential constant at these negative values the current remains practically constant for an indefinitely long time; this current is therefore sustained by a species present in the solution in large excess, namely, water itself, and not by some trace impurity in uracil. The anticipation of hydrogen discharge in the presence of uracil or of other organics depends to some extent on the state of the single-crystal face. It is less pronounced at a freshly cut and polished surface and increases progressively with an increasing use of the electrode, thus indicating that hydrogen evolution is favored by surface defects. The nature of the pretreatment of the electrode surface also has some effect; thus, annealing in a small hydrogen/air flame[12,13] has a slight beneficial influence. Conversely, the method of growth of the single-crystal electrode does not seem to have an appreciable effect on hydrogen discharge. Thus, no apparent difference was observed between electrodes prepared in our laboratory by the Bridgman method and an electrode prepared by the Czochralski method.

Charge Measurements at Short Electrolysis Times. Our strategy to investigate the kinetics of the 2D disorder−order phase transition yielding the chemisorbed condensed phase consisted in stepping the applied potential from a fixed initial value $E_i = -1.5$ V to different final values E lying over the potential range of the condensed phase. In Figure 2 the charge $Q(t,E)$ per unit surface following a given step is plotted against the time t elapsed from the instant of the step, for 5×10^{-4} M uracil and for different final potentials E. The $Q(t,E)$ vs t curves relative to the more positive final potentials E show two consecutive inflection points, which can be distinguished only with some difficulty because the slopes of the $Q(t,E)$ vs t curves at these points are close. These two inflection points correspond to a minimum and a subsequent maximum in the corresponding current vs time curves, the separation between minimum and maximum being small. Hence, the shape of the above $Q(t,E)$ vs t curves points to a combination of RA and PG. As the final potential E in the $Q(t,E)$ vs t curves of Figure 2 becomes progressively less positive, the inflection points vanish, and only a portion of roughly constant and positive slope is observed, which precedes the attainment of the time-independent limiting value of $Q(t,E)$. It is possible that the inflection points are no longer detected because the more rapid attainment of the limiting value of $Q(t,E)$ as observed at less positive E values causes these inflection points to be obliterated by the capacitive charge following the -1.5 V $\rightarrow E$ step, whose charge vanishes only after 0.01−0.02 s. For a constant final potential E, the rate at which the charge $Q(t,E)$ attains its maximum limiting value increases notably with an increase in the uracil concentration, c. This is clearly shown in Figure 3, which refers to a final potential $E = -0.1$ V; while for $c = 1 \times 10^{-4}$ M the second inflection point lies outside the time window of 0.6 s adopted in our chronocoulometric measurements, for $c = 6 \times 10^{-4}$ M the maximum limiting charge is already attained at 0.05 s. Hence, the kinetics of RA and PG can only be investigated over this relatively narrow concentration range.

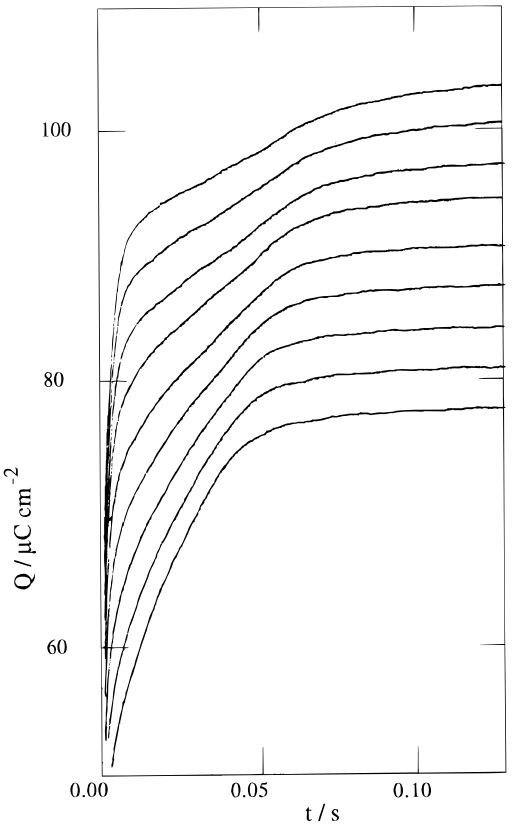

Figure 2. $Q(t,E)$ vs t curves of 5×10^{-4} M uracil from 0.05 M $KClO_4$ on Ag(111) as obtained by stepping the applied potential from −1.5 V/SCE to different final values E. Proceeding upward, the E values increase from −0.5 to −0.1 V by 50 mV increments.

The use of an initial potential E_i as negative as −1.5 V, where a moderate hydrogen evolution takes place even in the absence of uracil, requires an explanation. In fact, in Figure 1 the cyclic voltammogram as obtained in the presence of 2×10^{-4} M uracil merges with that in its absence at potentials ranging from ca. −1.0 V to ca. −1.25 V. This behavior leads to the conclusion that uracil molecules are completely desorbed at potentials negative to −1.0 V within the limits of sensitivity of cyclic voltammetry. On the other hand, at potentials negative to −1.25 V the presence of uracil causes an incipient hydrogen evolution, which in its absence takes place only at about −1.4 V. This strongly suggests that traces of uracil molecules, not detectable by electrochemical means but in a condition of catalyzing hydrogen evolution, are still adsorbed on surface defects even at a potential as negative as −1.3 V. This conclusion is supported by STM images obtained in our laboratory, which show the presence of unresolved material adsorbed along the steps at −1.3 V.[33] Unfortunately, no STM images can be obtained at still more negative potentials, due to the disturbing effect of hydrogen evolution; hence, it is not possible to ascertain by STM at which far negative potentials these traces of uracil molecules are completely removed from surface defects.

The above behavior is to be related to the observation that reproducible $Q(t,E)$ vs t curves with detectable inflections can only be obtained by adopting an initial potential E_i in the range from −1.4 to −1.6 V; practically identical results are also obtained by choosing initial potentials E_i more positive than −1.4 V, say −1.0 V, but only provided that the electrode surface is previously pretreated at a potential in the range from −1.4 to −1.6 V for no less than 20 s and the rest time at E_i before the positive potential step $E_i \rightarrow E$ is no longer than about 10 s. This behavior can be interpreted by considering that surface defects act as preferential adsorption sites on which uracil

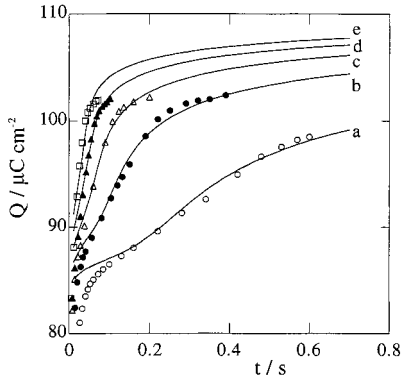

Figure 3. The points are $Q(t,E)$ vs t values as obtained on Ag(111) from 0.05 M $KClO_4$ solutions containing 1.8×10^{-4} (a), 3×10^{-4} (b), 4×10^{-4} (c), 5×10^{-4} (d), and 6×10^{-4} M (e) uracil by stepping from -1.5 to -0.1 V. The solid curves were calculated for the case of diffusion-controlled Frumkin adsorption with progressive PG (eqs 4, A9, A13, A20, and A21) by setting $\Delta\sigma_\theta = 25\ \mu$C cm^{-2}, $\Delta\sigma_S = 35\ \mu$C cm^{-2}, $K = 2 \times 10^3$ s$^{-3/2}$, $n = 5$, $\beta = 1 \times 10^3$ L mol^{-1}, and $a = -3.5$. The whole set of calculated curves was shifted along the vertical axis to achieve the best overlapping with the experimental curves: this shift compensates for the initial capacitive contribution to the charge density following the potential step from -1.5 to -0.1 V.

molecules remain adsorbed at potentials as negative as -1.3 V, even though the amount adsorbed is small enough as not to be detected by cyclic voltammetry. If these defects also act as nucleation centers, their initial occupation by uracil molecules will blur to some extent the polynucleation stage following the positive potential step. In this case the typical features of PG will only be revealed if these uracil molecules are completely desorbed by the application of a strongly negative potential. The fact that the choice of any initial potential E_i over the range from -1.4 to -1.6 V yields identical $Q(t,E)$ vs t curves with detectable inflections (apart from the obvious difference in the initial double-layer charge) indicates that at these E_i values no traces of adsorbed uracil molecules in a condition of affecting the kinetics of polynucleation are present on the electrode surface. The resulting $Q(t,E)$ vs t curves can therefore be compared with the predictions of models that assume the initial absence of adsorbed molecules in interpreting the kinetics of 2D phase transitions under potentiostatic conditions.

Differential Capacity Measurements. The constant limiting value of the charge $Q(t,E)$ in Figures 2 and 3 can be regarded as such only on the time scale of seconds and provided the solution is unstirred. On the time scale of minutes a gradual variation of the differential capacity C in time reveals the occurrence of a second 2D phase transition, yielding a further condensed phase henceforth referred to as phase II. On this time scale differential capacity measurements are definitely to be preferred to charge measurements, since they are much less sensitive to artifacts due to any electroactive impurities.[1] Curve a in Figure 4 is a typical C vs t curve at $E = -0.55$ V, as obtained by first keeping the electrode at $E_i = -1.5$ V for 20 s, by then stepping the applied potential to E, and by measuring C as a function of time from the instant of the potential step. The initial portion of this curve, up to the minimum, is analogous to those normally encountered in nucleation and growth processes, in that it has the shape of an inverted S. However, as distinct from normal nucleation and growth processes, after the minimum the differential capacity C increases again until it reaches a constant limiting value. A mild stirring of the solution accelerates the attainment of this limiting value by compressing the C vs t curve into a narrower time range without altering its shape to an appreciable extent (see curve b in Figure 4). The time required to attain the limiting C value also depends to some

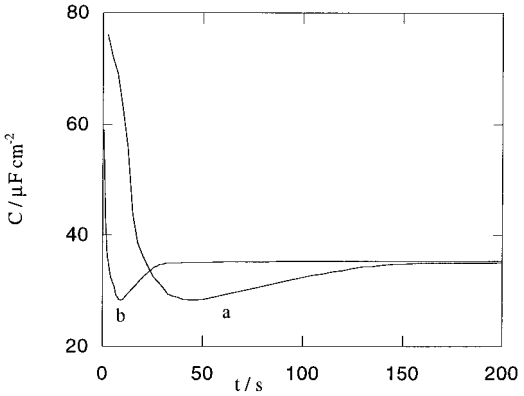

Figure 4. C vs t curves of 5×10^{-4} M uracil from 0.05 M $KClO_4$ on Ag(111) at $E = -0.55$ V obtained as described in the text both in the absence (a) and in the presence (b) of a mild stirring of the solution.

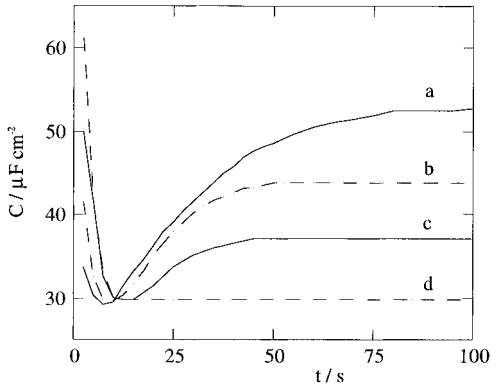

Figure 5. C vs t curves on Ag(111) at -0.55 V as obtained under mild stirring from 0.05 M $KClO_4$ solutions containing 1×10^{-4} (a), 3×10^{-4} (b), 5×10^{-4} (c), and 6×10^{-4} M (d) uracil.

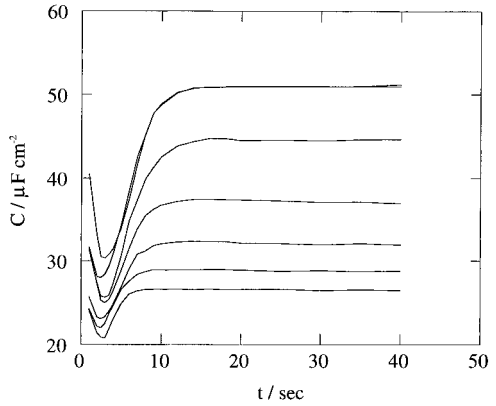

Figure 6. C vs t curves of 1×10^{-4} M uracil from 0.05 M $KClO_4$ on Ag(111) as obtained under mild stirring at different applied potentials E. Proceeding upward, the E values decrease from -0.3 to -0.6 V by -50 mV steps. The upper portions of the C vs t curves at -0.55 and -0.6 V practically coincide.

extent on the state of the electrode surface: this time was normally found to be longer at a freshly cut electrode than at an electrode that had been used several times. Figure 5 shows a series of C vs t curves for different bulk concentrations of uracil as obtained at $E = -0.55$ V under mild stirring. It can be seen that an increase in c from 1×10^{-4} to 6×10^{-4} M causes the limiting value of the differential capacity to decrease up to the disappearence of the minimum in the C vs t curve. Figure 6 shows a series of C vs t curves for 1×10^{-4} M uracil at different applied potentials E, as obtained once again under mild stirring in order to accelerate the attainment of the limiting value. This value increases with a negative shift of E from -0.3 to -0.6 V, thus exhibiting a trend analogous to that of

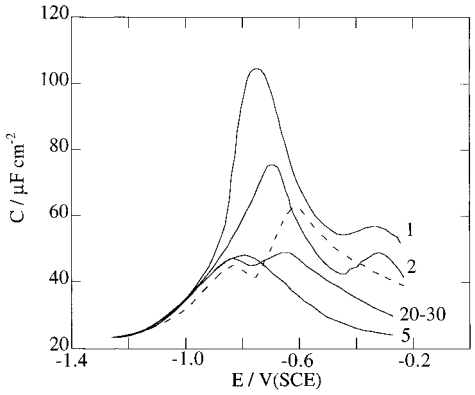

Figure 7. *C* vs *E* curves of 3×10^{-4} M uracil from 0.05 M $KClO_4$ on Ag(111) as obtained under mild stirring at different times *t* from the instant of the -1.5 V $\rightarrow$ *E* potential step by the procedure described in the text; numbers on each curve denote *t* values in s.

the differential capacity of 0.05 M $KClO_4$ alone (see, for example, Figure 1 in ref 31). Figure 7 shows the *C* vs *E* curves of 3×10^{-4} M uracil for different values of the time *t* elepased from the instant of the -1.5 V $\rightarrow$ *E* step: they were obtained from a series of *C* vs *t* curves recorded by stepping from -1.5 V to a more positive *E* value, which was increased progressively by 25 mV steps, and by then plotting the resulting capacity values at a given time against *E*. It is apparent that for $t > 20$ s the *C* vs *E* curves attain a stationary behavior and merge with the curve of 0.05 M $KClO_4$ alone at potentials negative to -1.1 V.

One possible, trivial explanation for the capacity increase in Figures 4−6 might be the coadsorption of some highly adsorbable trace impurity, requiring a long time to displace the uracil molecules of the condensed phase II from the electrode surface. To discard this possibility, *C* vs *t* curves in the absence of uracil under otherwise identical conditions were recorded for 10 min, the maximum time period adopted in our differential capacity measurements; the resulting *C* vs *t* curves were found to be almost horizontal, with only a very slight negative slope. To exclude the remaining possibility of some impurity in the uracil, samples from different sources and subject to a different number (two or three) of recrystallizations prior to use were employed; in all cases *C* vs *t* curves of the same shape were obtained. The dependence of the time scale of the *C* vs *t* curves on the state of the Ag(111) face could also be hardly explained by the effect of the diffusion-controlled adsorption of a highly adsorbable trace impurity. Conversely, the constancy in the shape of the *C* vs *t* curves, including the minimum and limiting values of *C*, as their time scale is contracted by stirring or by a prolonged use of the electrode, suggests that these curves are due to a sequence of events involving the sole uracil.

Discussion

The Short-Time Behavior. This behavior, with particular regard to the concentration dependence of the *Q* vs *t* transients, will be explained by the model decribed in Appendix I, which accounts for the unavoidable diffusion of uracil molecules toward the electrode, their random adsorption (RA), and progressive polynucleation and growth (PG) of the randomly adsorbed uracil molecules. The rate of the overall process is considered to be controlled by diffusion of the uracil molecules from the bulk solution toward the electrode and by PG, whereas RA is regarded as in quasi-equilibrium. RA is assumed to satisfy the Langmuir isotherm or, alternatively, the Frumkin isotherm.

It will also be assumed that adsorbate−adsorbate interactions, which are mainly responsible for PG, and adsorbate−substrate interactions, which are responsible for chemisorption, affect uracil adsorption independently from each other. This assumption is justified when adsorbate−substrate interactions are not strictly directional. That this is often the case is demostrated by the observation that even simple monoatomic adsorbates such as halide ions yield overlayers that, albeit structurally well ordered, are incommensurate with respect to the substrate and exhibit a continuous compression with increasing potential when examined by in situ surface X-ray scattering.[34−37] Moreover, STM images of halide ions adsorbed at single-crystal faces reveal the presence of structurally ordered islands at potentials slightly negative to those at which the surface becomes fully covered by an overlayer;[38] the same conclusions are suggested by the potential dependence of the intensity of the diffraction peaks in surface X-ray scattering.[34] Moreover, the preference of bromide adlayers on Au(100) for a structure close to hexagonal rather than the square $c(2\times2)$ structure, where the adatoms would reside in higher coordinated 4-fold hollow sites, suggests that the elastic interactions between these relatively large adsorbate atoms (ions), which favor hexagonal packing, are more significant that the adsorbate−substrate interaction energy difference between the two structures.[37] This points to the essential role played by adsorbate−adsorbate interactions even in the case of partial charge transfer from the adsorbate to the substrate. In the case of an adsorbed uracil molecule, whose cross sectional area covers more than one elementary cell of the underlying substrate, the lack of directionality of any adsorbate−substrate interactions is even more justified; this is further supported by STM images showing the presence of islands of uracil molecules on Ag(111).[33]

The present model refers to a "quasi-ideal" single-crystal face with only point defects (adatoms, vacancies, kinks) and monodimensional defects (monoatomic steps), the remaining area consisting of regularly structured, uniform terraces. Under these conditions areas covered by randomly adsorbed molecules cannot coexist with areas covered by clusters of a condensed phase at equilibrium, other than at a single potential (the transition potential) or, at most, over a very narrow potential range.[30] Hence, in the potential region of stability of the condensed phase, randomly adsorbed molecules will tend to organize themselves spontaneously into "liquid-like" or "quasi-solid-like" clusters, first subcritical and then supercritical in size. Such a PG process is expected to proceed at a lower rate than the precursor RA process, since self-organization normally requires the complete squeezing out of the adsorbed water molecules from the condensed clusters and a favorable orientation of the adsorbed molecules, which may sometimes be accompanied by hydrogen-bond formation between adjacent solute molecules, as postulated by de Levie and Wandlowski[39] for uracil and its derivatives. In this case the randomly adsorbed solute molecules will be more readily available for incorporation into condensed clusters than solute molecules diffusing from the bulk solution, unless surface diffusion is strongly hindered. In fact, the randomly adsorbed molecules are already present on the electrode surface in an appreciable amount before PG proceeds to a detectable extent; conversely, the solute molecules diffusing from the bulk must exactly hit the periphery of the clusters[27] in order to grow them without being previously adsorbed in a random way. Incorporation of the latter molecules on top of the clusters[30] will be excluded, since it seems energetically unfavored.

As concerns polynucleation, it will be considered to be "heterogeneous", in that adatoms; kinks and monoatomic steps will be regarded as preferential sites not only for random adsorption but also for nucleation. In other words these surface

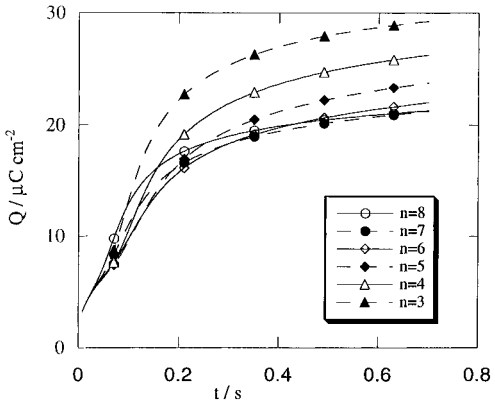

Figure 8. Q vs t curves calculated in the case of diffusion-controlled Frumkin adsorption with progressive PG (eqs 4, A9, A13, A20, and A21) for $c = 3 \times 10^{-4}$ M, n ranging from 3 to 8, and the other parameters as in Figure 3.

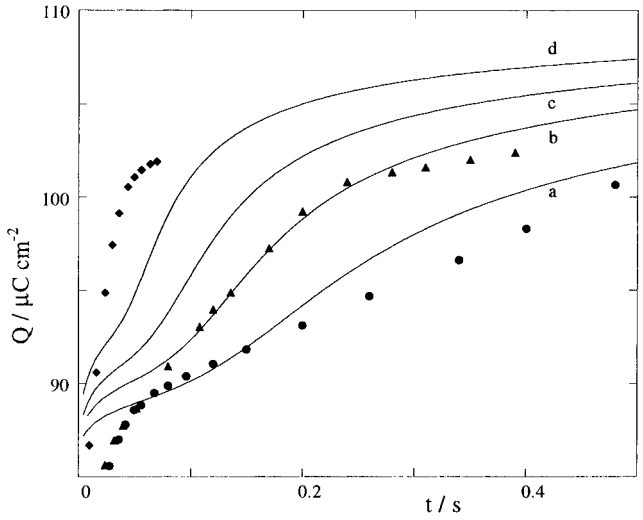

Figure 9. The points are the same experimental Q vs t values as in Figure 3 for 1.8×10^{-4} (●), 3×10^{-4} (▲), and 6×10^{-4} M (◆) uracil. The solid curves were calculated for the case of diffusion-controlled Langmuirian adsorption with progressive PG (eqs 4, A9, A13, and A16-A18) for $c = 1.8 \times 10^{-4}$ (a), 3×10^{-4} (b), 4×10^{-4} (c), and 6×10^{-4} M (d) by setting $\Delta\sigma_\theta = 15\ \mu$C cm^{-2}, $\Delta\sigma_S = 25\ \mu$C cm^{-2}, $K = 2 \times 10^3$ s$^{-3/2}$, $n = 5$, and $\beta = 3 \times 10^3$ L mol^{-1}. The whole set of calculated curves was shifted along the vertical axis to achieve the best overlapping between the calculated and the experimental curve relative to $c = 3 \times 10^{-4}$ M.

defects will be regarded as nucleation centers, just as the mononucleation at a mercury electrode is triggered at the lumen of the capillary,[40] which constitutes the only singularity on the electrode surface. The "initial" number N_0 of nucleation centers per unit surface will therefore be regarded as fixed and relatively high. In this connection two alternative situations will be considered, depending on whether the maximum number of nuclei that are formed around the available nucleation centers before the electrode surface is fully covered by the condensed phase is much less than N_0 or not. In the former case the time-dependent number $N(t)$ of nuclei is constantly much less than N_0, a familiar assumption in the treatment of PG. In the latter case the progressive decrease in time of the still "unoccupied" nucleation centers, $N_0 - N(t)$, must be accounted for: this case will be referred to as progressive polynucleation with decay of the nucleation centers. In both the above cases, but especially in the former one, the problem of incorporation of still "unoccupied" nucleation centers into clusters growing around already "occupied" ones arises: this effect, called "ingestion effect",[27,41,42] will also be accounted for.

The calculation of the Q vs t curves for any of the situations to be examined requires (i) the diffusion coefficient D of uracil to account for its diffusion; (ii) the maximum surface concentration Γ_m and the adsorption coefficient β of uracil to account for its RA; and (iii) a single parameter $K = 2k_R(\pi N_0 k_N)^{1/2}$, which embodies the rate constant k_N for nucleation as well as that, k_R, for the radial growth of clusters, to account for progressive PG. Moreover, RA obeying the Frumkin isotherm, rather than the Langmuir isotherm, requires the Frumkin interaction factor a to be specified in addition to the adsorption coefficient β. Finally, consideration of the ingestion effect requires the k_N value to be explicitly specified. The diffusion coefficient $D = 7.2 \times 10^{-6}$ cm^2 s^{-1} [43] and the maximum surface concentration $\Gamma_m = 4.5 \times 10^{-10}$ mol cm^{-2} [44] of uracil in the dilute phase were taken from the literature.

All cases examined also require the specification of the number n of solute monomers composing a nucleus, namely, the minimum cluster of monomers having a greater tendency to grow than to dissolve. For all these cases and for all sets of parameters that may comply with the experimental behavior, a common feature emerges as n is progressively increased. This feature, which is exemplified by Figure 8 relative to diffusion-controlled Frumkin adsorption with progressive PG, consists in a gradual shift of the calculated Q vs t curves toward longer times as n is increased up to 5−6 under otherwise identical conditions, followed by an inversion in the trend with a further increase in n. Hence, our model points to an activationless incorporation of solute molecules into clusters consisting of more than about 5 monomeric units; namely, it predicts a 5-meric nucleus. In what follows n will therefore be constantly set equal to 5.

If we exclude the capacitive charge density that is required to charge the interphase following the potential step $E_i \rightarrow E$ and that flows within 10−20 ms from the instant of the potential step, the charge density $Q(t)$ flowing at the final potential E is given by

$$Q(t) = \Delta\sigma_\theta\theta(t) + \Delta\sigma_S S(t) \quad \text{with} \quad \Delta\sigma_\theta \equiv \sigma_\theta - \sigma_0; \quad \Delta\sigma_S = \sigma_S - \sigma_0 \quad (4)$$

Here σ_0, σ_θ, and σ_S are the charge densities at E of an electrode free of adsorbed molecules, fully covered by randomly adsorbed surfactant molecules, and fully covered by the condensed phase, respectively. In practice, the parameters $\Delta\sigma_\theta$ and $\Delta\sigma_S$ cannot be regarded as entirely adjustable, since they are dictated by the experimental conditions.

Figure 9 shows Q vs t curves calculated for different uracil concentrations upon assuming Langmuirian adsorption with progressive PG (case 1 in Appendix I). The adjustable parameters K and β were chosen in such a way as to obtain the best agreement with experiment for the intermediate concentration $c = 3 \times 10^{-4}$ M. For comparison, this figure shows the experimental curves for $c = 1.8 \times 10^{-4}$, 3×10^{-4}, and 6×10^{-4} M. It is apparent that this model predicts a concentration dependence of the Q vs t curves that is lower than that observed experimentally. No possible choice of the parameters K and β can account satisfactorily for this experimental dependence. To improve the agreement between calculated and experimental Q vs t curves, we must postulate a higher rate of increase of θ with c, such as that predicted by a Frumkin isotherm with an attractive interaction factor a. Figure 3 shows indeed that a diffusion-controlled Frumkin adsorption with progressive PG (case 2 in Appendix I) with an interaction factor $a = -3.5$ accounts satisfactorily for both the shape and the concentration dependence of all the experimental Q vs t curves. The fact

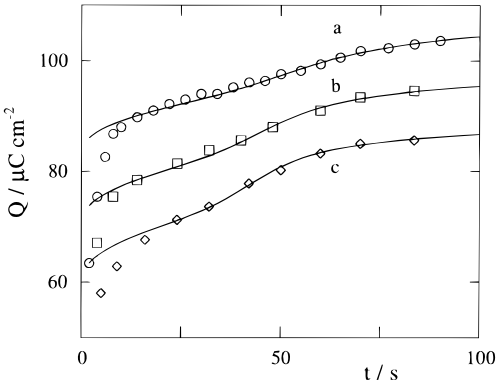

Figure 10. The points are the same Q vs t values as in Figure 2 for $E = -0.1$ (a), -0.2 (b), and -0.3 V (c). The corresponding solid curves were calculated as in Figure 3 by using the same parameters adopted therein, with the only exception of β, which was ascribed the values 1×10^3, 1.5×10^3, and 2×10^3 L mol^{-1}, respectively. The calculated curves were shifted along the vertical axis so as to achieve the best overlapping with the experimental curves.

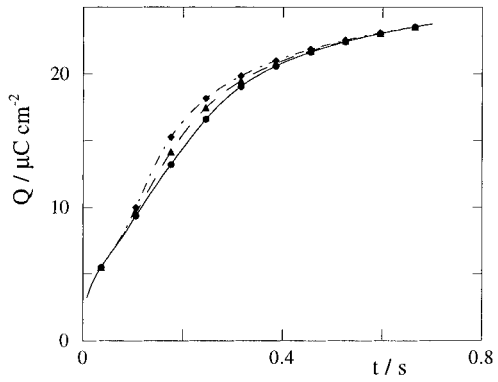

Figure 11. Q vs t curves calculated for the case of diffusion-controlled Frumkin adsorption with progressive PG with decay of the nucleation centers (eqs 4, A9, A20, A21, and A23) for $k_N = 100$ (◆), 2000 (▲), and 3000 s^{-1} (●), $c = 3 \times 10^{-4}$ M, and the other parameters as in Figure 3.

that the experimental $Q(E,t)$ vs t curves in Figure 2 attain their maximum limiting value at shorter times as E becomes progressively more negative can be explained by a concomitant increase in the adsorption coefficient β for the randomly adsorbed uracil molecules. The maximum adsorptivity of randomly adsorbed organic molecules is normally attained in the proximity of the potential of zero charge in the absence of surfactants, which equals -0.745 V for the Ag(111) face;[31,45] it is therefore quite reasonable to expect an increase in β when shifting from -0.1 to -0.5 V. In Figure 10 the experimental $Q(E,t)$ vs t curves of Figure 2 for $E = -0.1$, -0.2, and -0.3 V are compared with curves calculated by using the same parameters as adopted in Figure 3, with the only obvious exception of β, which was gradually increased in passing from -0.1 to -0.3 V. Even though no attempt was made to modify the $\Delta\sigma_\theta$ and $\Delta\sigma_S$ values with varying E, the simple increase in β is sufficient to provide a qualitative justification for the experimental trend, and in particular for the shift of the inflection points toward shorter times.

Accounting for the ingestion effect (case 4 in Appendix I) while maintaining the same parameters as adopted in Figure 3 leads only to a very modest decrease in the upper portion of the resulting calculated Q vs t curves, which does not permit us to appreciate its relevance from a comparison with the experimental curves. Consideration of progressive polynucleation with decay of the nucleation centers (case 3 in Appendix I) requires the introduction of a further adjustable parameter, i.e. the rate constant k_N for nucleation. It is apparent from Figure 11 that a progressive increase in this parameter while keeping K constant (i.e., while decreasing the rate constant k_R for radial growth) tends to reduce, and ultimately to almost eliminate, the two intermediate inflection points in the calculated Q vs t curves. Introduction of this further effect may slightly improve agreement with experiment. However, in our opinion the agreement between calculated and experimental curves in Figure 3 is already sufficiently satisfactory as not to justify a slight improvement at the expense of a further adjustable parameter.

Long-Time Behavior. The initial sigmoidal, descending branch of the C vs t curve a in Figure 4 is ascribed to a 2D phase transition from the condensed phase formed during the short-time charge transients (henceforth referred to as phase I) to a further condensed phase (phase II) characterized by a greater thickness. In this respect we may envisage a transition from a flat to a tilted or vertical orientation of the adsorbed uracil molecules. Incidentally, according to Wandlowski,[12] the mixing of the d-orbitals of the Ag surface atoms with the nonbonding orbitals of the uracil molecules may actually favor a tilted orientation. Following Pospísil and Wandlowski,[18,24] we will explain the subsequent increase in capacity by the nucleation and growth of water clusters within phase II. According to models of interfacial water molecules against a charged wall developed in our laboratory,[46,47] adsorbed water molecules tend to be squeezed out of the adsorbed layer when they are surrounded by adsorbed solute molecules, which hinder their H-bonding with the adjacent adsorbed and nonadsorbed water molecules. In the present case the water molecules that initially penetrate the adsorbed layer of uracil molecules during the I → II transition, due to the decreased area occupied by the reorienting surfactant molecules, are severely hindered from forming H-bonds between themselves and with the overhanging water molecules of the solution phase. Hence, they will tend either to be squeezed out of the adsorbed layer or to aggregate: the former tendency will prevail more over the latter the higher the uracil bulk concentration c. We may therefore envisage the attainment of a steady-state situation, which depends on the c value and which may explain the attainment of a time-independent capacity at sufficiently long times (see Figures 4−6).

To model this complex situation we will make the following simplifying assumptions.

(1) When the I → II transition starts to take place, the electrode surface is already fully covered by the condensed phase I, so as to permit us to write

$$S_I + S_{II} = 1 \tag{5}$$

where S_I and S_{II} are the surface coverages by the two phases I and II; since the third condensed phase consisting of water aggregates may exist only within phase II, S_{II} defines the surface coverage by phase II even when it incorporates water aggregates.

(2) The nucleation of phase II is considered to be homogeneous and to be partially fed by uracil molecules from the bulk solution. In view of the complexity of the situation, we will just adopt the well-known approximation for "progressive nucleation", by regarding the nucleation rate $v_{II,N}$ of phase II as constant in time

$$dN_{II}/dt \equiv v_{II,N} = \text{constant} \tag{6}$$

(3) The nucleation of water clusters within phase II is also considered to be homogeneous in nature and to be mainly fed by the nonadsorbed water molecules of the solution phase. Since the bulk concentration of water molecules is practically constant,

it can be embodied in the rate constant $k_{w,N}$ for the nucleation of water clusters. The corresponding nucleation rate is then written

$$dN_w/dt \equiv \upsilon_{w,N} = \text{constant} \quad (7)$$

according to the approximation for progressive nucleation.

(4) The uracil molecules are assumed to be adsorbed randomly into the water aggregates according to the same Frumkin isotherm valid for the short-time behavior, tending to oppose their expansion by colliding with their periphery. The rate $\upsilon_{w,R}$ of radial growth of the water clusters is therefore determined by two contrasting phenomena: the collisions of water molecules with the edges of the water clusters, which tend to expand the clusters, and the collisions of the randomly adsorbed uracil molecules, which tend to contract them. If we assume that the above collisions involve exclusively adsorbed molecules of either water or uracil, the rates of increase of the area and of the radius R_w of a circular cluster are given by

$$d(\pi R_w^2)/dt = (2\pi R_w)[k_e(1-\theta) - k_c\theta] \Rightarrow$$
$$\upsilon_{w,R} \equiv dR_w/dt = k_e - (k_e + k_c)\theta \quad (8)$$

where k_e and k_c are the rate constants for the expansion and for the contraction of the water clusters, respectively. As a matter of fact, the great abundance of nonadsorbed water molecules in the proximity of the electrode surface may well justify a major contribution of these "bulk" water molecules to the expansion of the water clusters, via their collisions with the cluster edges. However, even in this case eq 8 is still formally valid, with the simple replacement of the composite rate constant ($k_e + k_c$) by k_c in the expression for $\upsilon_{w,R}$.

The maximum limiting value attained by the surface coverage S_w by the water aggregates is obviously S_{II}. The differential capacity C at a given potential will therefore be given by

$$C = C_I(1 - S_{II}) + C_{II}(S_{II} - S_w) + C_wS_w \quad (9)$$

where C_I, C_{II}, and C_w are the capacities per unit surface of the condensed phases I and II and of the water aggregates. The C_I value is provided by dQ_{lim}/dE, where Q_{lim} is the time-independent, limiting value of Q as attained in the time window of 0.6 s adopted in the chronocoulometric measurements, when the electrode becomes fully covered by the condensed phase I; at the potential of -0.55 V chosen in Figure 4, dQ_{lim}/dE is $\sim$90 μF cm^{-2}. The C_{II} value is provided by the constant minimum value attained by C at sufficiently high uracil concentrations ($\sim$27 μF cm^{-2} at -0.55 V). C_w can be equated to the capacity of the surfactant-free electrode (54 μF cm^{-2} at -0.55 V) only as a first approximation. In fact, as the water aggregates become sufficiently large, the adsorbed water molecules are expected to form hydrogen bonds with the adjacent water molecules of the bulk solution phase and to "dissolve" randomly adsorbing uracil molecules.

Figure 11 shows C vs t curves calculated on the basis of this model by the procedure outlined in Appendix II. The calculation requires the use of three adjustable parameters: $K_{II} \equiv 2\upsilon_{II,R}(\pi\upsilon_{II,N})^{1/2}$, $K_w \equiv 2k_e(\pi\upsilon_{w,N})^{1/2}$, and $\zeta \equiv k_c/k_e$, where $\upsilon_{II,R}$ is the rate of radial growth of the clusters of phase II. In practice, K_{II} controls the rate of nucleation and growth of phase II from phase I, K_w that of the water clusters from phase II, and ζ the steady-state value of the differential capacity. Since the time scale of the experimental C vs t curves depends on the stirring rate and, to a minor extent, on the state of the electrode surface (see Figure 4), the time scale of the corresponding calculated curves in Figure 12 is also kept arbitrary. By so doing, to reproduce the shape of the experimental C vs t curves only two adjustable parameters are required, say K_w/K_{II} and ζ/K_{II}. A fairly good agreement between the shapes of the calculated and experimental curves relative to the different concentrations employed is attained by setting $K_w/K_{II} = 0.1$ and $\zeta/K_{II} = 7$ s$^{3/2}$, as appears by comparing Figures 5 and 12. Note that the K_w/K_{II} ratio is less than unity, since the rate of formation of the water clusters within phase II must be necessarily lower than the rate of formation of phase II from phase I, in order to predict a minimum in the C vs t curves.

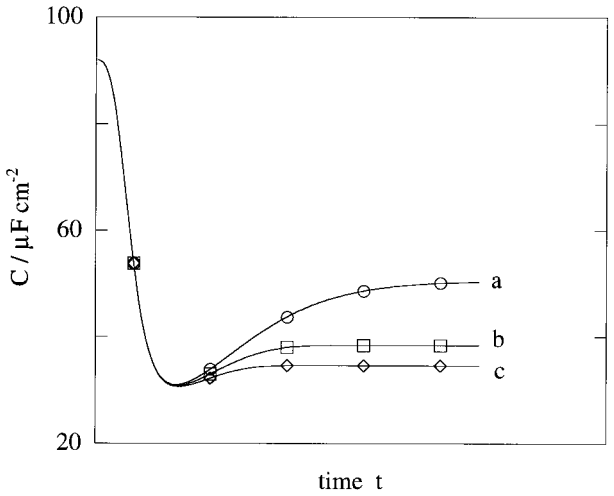

Figure 12. C vs t curves calculated as described in the text from eqs 9, A25, and A27−A30 for $\beta = 1 \times 10^3$ L mol^{-1}, $a = -3.5$, $K_w/K_{II} = 0.1$, $\zeta/K_{II} = 7$ s$^{3/2}$, and $c = 1 \times 10^{-4}$ (a), 3×10^{-4} (b), and 6×10^{-4} M (c).

Figure 4 shows that an increase in the stirring rate compresses the time scale of the experimental C vs t curves while retaining their shape. In this connection it must be noted that in the time scale of all our differential capacity measurements the diffusion step can practically be regarded in equilibrium. In fact, the time τ required to attain the maximum surface concentration Γ_m under limiting conditions for pure diffusion, namely, when the volume concentration of the surfactant in the immediate vicinity of the electrode is negligibly small with respect to its bulk value c, is given by $\pi\Gamma_m^2/(4Dc^2)$ in view of the Cottrell equation; for $D = 7.2 \times 10^{-6}$ cm^2 s^{-1} [43] and $\Gamma_m = 4.5 \times 10^{-10}$ mol cm^{-2},[44] τ equals 2.2 s when $c = 10^{-4}$ M and decreases very rapidly with an increase in c. This implies that in the long-time behavior the uracil molecules that cross an ideal geometrical surface in the proximity of the electrode in one direction are practically equal in number to those that cross it in the opposite direction in the same time, independent of whether the solution is stirred or not. However, stirring increases such a number and hence the frequency of the collisions of both uracil and water molecules with the adsorbed layer: this will accelerate the reorientation of the adsorbed uracil molecules via a more rapid insertion of bulk water and uracil molecules into the voids left free by the more vertically oriented uracil molecules, as well as the attainment of the steady-state size of the water clusters. In other words, stirring increases the preexponential frequency factors of all steps involved in the nucleation and growth of phase II and of water clusters within phase II. As a first approximation, the effect of stirring can therefore be formally accounted for by increasing the rates $\upsilon_{II,R}$, $\upsilon_{II,N}$, and $\upsilon_{w,N}$ and the rate constants k_e and k_c by the same factor f. By so doing the calculated C vs t curves in Figure 13 are obtained, which simulate the experimental behavior.

Acknowledgment. The authors are grateful to Prof. D. M. Kolb and to Drs. M. H. Hölzle and Th. Wandlowski for

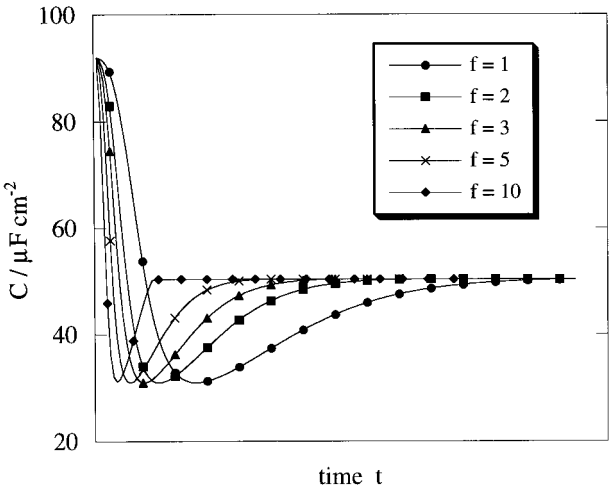

Figure 13. C vs t curves calculated for $c = 1 \times 10^{-4}$ M, $K_w = 0.2f^{3/2}$ $s^{-3/2}$, $K_w/K_{II} = 0.1$, $\zeta = 14$ and for different values of the factor f by which all the rates $v_{II,R}$, $v_{II,N}$, $v_{w,N}$, k_e, and k_c are multiplied to simulate the effect of stirring.

providing them with the manuscripts of their works on 2D condensation on gold and silver single-crystal faces and for helpful suggestions. The financial support of the Ministero dell'Universita' e della Ricerca Scientifica e Tecnologica and of the Consiglio Nazionale delle Ricerche is gratefully acknowledged.

Appendix I

The extended area S_x, namely, the hypothetical area per unit surface which would be covered by the growing clusters if their overlapping could be ignored, is expressed by the quite general relationship[41]

$$S_x = g\int_0^t \mathrm{d}y[\int_y^t v_R(z)\,\mathrm{d}z]^2 v_N(y) \qquad \text{(A1)}$$

with

$$v_R(t) \equiv \mathrm{d}R/\mathrm{d}t; \quad v_N(t) \equiv \mathrm{d}N/\mathrm{d}t \qquad \text{(A2)}$$

Here $\mathrm{d}N/\mathrm{d}t$ is the rate of nucleation, $\mathrm{d}R/\mathrm{d}t$ is the rate of radial growth of the two-dimensional clusters, and g is a geometrical factor that takes the value π in the simplest case of a circular cluster and may be given a different value to account approximately for a different shape. Henceforth we will constantly refer to circular clusters for simplicity.

In the framework of the present model the nucleation rate will be obtained by considerating that the formation of a critical cluster (nucleus), assumed to be n-meric, results from n consecutive steps: the first step involves the aggregation of a monomer to a nucleation center, whereas any subsequent mth step, with $1 < m \leq n$, involves the incorporation of a monomer into a $(m-1)$-meric cluster. All m-meric clusters, with $m < n$, have a greater tendency to dissolve than to grow. Hence, to ensure nucleation and growth, all steps preceding the nth step must be necessarily regarded as bidirectional. Conversely, the nth step, which yields the critical cluster, as well as the subsequent steps, may well be regarded as unidirectional.[29] For simplicity, we will assume that the backward and forward rates of the first $n-1$ steps are much greater than the corresponding net rates, so as to permit us to regard these steps as in quasi-equilibrium. With this assumption the nucleation rate $\mathrm{d}N/\mathrm{d}t$ is proportional to θ^n, where θ is the surface coverage by the randomly adsorbed molecules, at least as long as the number N of nuclei is much less than that, N_0, of the initial nucleation centers. If this is not the case, the constraint imposed by a finite number of nucleation centers will be approximately accounted for by introducing the multiplying factor $(N_0 - N)$ into the expression for the nucleation rate. Whence

$$\mathrm{d}N/\mathrm{d}t = k_N(N_0 - N)\theta^n \qquad \text{(A3)}$$

where k_N is the rate constant for nucleation. Integration of eq A3 yields

$$N = N_0[1 - \exp(-k_N\int_0^t \theta^n\,\mathrm{d}t)] \qquad \text{(A4)}$$

Subsequent differentiation with respect to time yields

$$\frac{\mathrm{d}N}{\mathrm{d}t} = N_0 k_N \theta^n \exp[-k_N\int_0^t \theta^n\,\mathrm{d}t] \qquad \text{(A5)}$$

This is the expression for the rate of progressive polynucleation with decay of the nucleation centers. If the rate constant k_N is low enough to justify an expansion of the exponential of eq A4 arrested at the second term, differentiation of the resulting expression for N yields

$$\mathrm{d}N/\mathrm{d}t = N_0 k_N \theta^n \qquad \text{(A6)}$$

Apart from the time-dependent θ^n factor, this is the analogue of the nucleation rate for the so-called progressive nucleation. If we wish to account for a possible "ingestion effect",[27,41,42] eq A6 is modified as follows:

$$\mathrm{d}N/\mathrm{d}t = N_0 k_N \theta^n (1 - S) \qquad \text{(A7)}$$

The rate of radial growth is obtained by considering that the rate of increase, $\mathrm{d}A/\mathrm{d}t$, of the area of a supercritical cluster, regarded as circular for simplicity, is proportional to the frequency of the impacts of the randomly adsorbed solute molecules with the cluster periphery.[29] Hence

$$\mathrm{d}A/\mathrm{d}t = \mathrm{d}(\pi R^2)/\mathrm{d}t = 2\pi R\,\mathrm{d}R/\mathrm{d}t = k_R(2\pi R)\theta \Rightarrow \mathrm{d}R/\mathrm{d}t = k_R\theta \qquad \text{(A8)}$$

from which it follows that the rate of increase of the cluster radius is proportional to θ.

To avoid the overlapping of the growing clusters, Avrami's relationship[21] between the extended area S_x of the condensed phase and its effective area S is employed:

$$\mathrm{d}S/\mathrm{d}t = (1 - S)\,\mathrm{d}S_x/\mathrm{d}t \qquad \text{(A9)}$$

Note that Bosco and Rangarajan's expression of eq 3 is not employed, because according to our model the randomly adsorbed molecules do not decrease the surface area at the disposal of the condensed phase, since they are available for incorporation into this phase. Conversely, the area per unit surface available for random adsorption is indeed decreased by the presence of the condensed phase and hence is given by $(1 - \theta - S)$, as in eq 1.

By changing the integration variables, eq A1 can be written

$$S_x = g\int_0^t \mathrm{d}(t-y)[\int_0^{t-y} v_R(z-y)\,\mathrm{d}(z-y)]^2 v_N(t-y) \qquad \text{(A10)}$$

Differentiation with respect to t yields

$$\sqrt{\frac{S_x'}{g v_N(t)}} = \int_0^t v_R(u)\,\mathrm{d}u \qquad \text{(A11)}$$

with $S'_x \equiv dS_x/dt$. A further differentiation with respect to t leads to the expression

$$\frac{d^2S_x}{dt^2} \equiv S''_x = 2v_R(gS'_x v_N)^{1/2} + S'_x\frac{v'_N}{v_N} \quad \text{with} \quad v'_N \equiv \frac{dv_N}{dt} \quad \text{(A12)}$$

which will be applied to the following cases.

Case 1. Diffusion-Controlled Langmuirian Adsorption with Progressive PG. In this case $v_N \equiv dN/dt$ and $v_R \equiv dR/dt$ are expressed by eqs A6 and A8; their substitution into eq A12 yields

$$S''_x = K\sqrt{S'_x}\theta^{(n/2+1)} + nS'_x\theta'/\theta \quad \text{(A13)}$$

with

$$K \equiv 2k_R(gN_0k_N)^{1/2}; \quad \theta' \equiv d\theta/dt \quad \text{(A14)}$$

To solve the present problem, expressions for θ and θ' must be derived. According to the diffusion-layer approximation,[49,50] diffusion-controlled Langmuirian adsorption is expressed by the equation

$$D\int_0^t\left(\frac{\partial c}{\partial x}\right)_{x=0} dt \cong D\int_0^t \frac{c-\bar{c}}{\sqrt{\pi Dt}}\,dt = \Gamma = \Gamma_m(1-S)\frac{\beta\bar{c}}{1+\beta\bar{c}} \quad \text{(A15)}$$

where D and β are the diffusion coefficient and the coefficient for random adsorption of the surfactant, and $\bar{c}$ is its volume concentration in the immediate vicinity of the electrode surface. In this equation account has been taken of the fact that in the presence of the condensed phase the maximum surface concentration equals $\Gamma_m(1 - S)$. The adsorption isotherm on the right-hand side of eq A15 is consistent with the kinetic expression of eq 1, as is readily verified by setting $d\theta/dt = 0$ in this equation, so as to refer to the condition of adsorption equilibrium, and by noting that $k_{ads}/k_{des} = \beta$. According to the diffusion-layer approximation, the rate of change of $\bar{c}$ with time is assumed to be small with respect to that of $t^{-1/2}$, so as to permit us to bring $(c - \bar{c})$ outside the integral sign in eq A15: in general this approximation involves an error less than 8%.[50]

By so doing, after simple algebraic manipulations we obtain

$$\theta = (1-S)\psi\rho/(1+\psi\sigma) \quad \text{with} \quad \psi \equiv \beta c; \quad \rho \equiv \bar{c}/c \quad \text{(A16)}$$

with

$$\rho = \frac{-b+\sqrt{b^2+4\psi}}{2\psi}; \quad b = 1-\psi+\xi\psi(1-S); \quad \xi = \frac{\pi^{1/2}\Gamma_m}{2c(Dt)^{1/2}} \quad \text{(A17)}$$

In the limiting case in which $S \rightarrow 1$, eq A17 predicts that $\bar{c} \rightarrow c$. In other words $\bar{c}$, after decreasing with respect to its bulk value c, increases again due to the gradual replenishment of the depletion due to the initial random adsorption. The expression for θ' is now readily obtained by differentiating the expression of $\theta = \theta[S(t),\rho(t)]$ in eq A16:

$$\theta' = -\frac{\psi\rho}{1+\psi\rho}S' + (1-S)\frac{\psi}{(1+\psi\rho)^2}\left[\frac{\xi\psi\rho}{(2\psi\rho+b)}\left(S' + \frac{1-S}{2t}\right)\right] \quad \text{(A18)}$$

The three differential equations (A9), (A13), and (A18), with θ and ρ expressed by eqs A16 and A17, can be readily solved numerically by the fourth-order Runge−Kutta method, with the conditions $\theta = S = S'_x = 0$ for $t = 0$. The resulting values of θ and S as a function of t are then introduced into eq 4 to obtain the calculated curves of Q vs t.

Case 2. Diffusion-Controlled Frumkin Adsorption with Progressive PG. This case differs from case 1 exclusively for the expressions of θ and θ'. The dependence of θ upon $\bar{c}$ is expressed by the following modified version of the well-known Frumkin isotherm:

$$\beta\bar{c} = \theta\exp(a\theta)/(1-\theta-S) \quad \text{(A19)}$$

where a is the Frumkin interaction factor. In the framework of the diffusion-layer approximation, by considerations analogous to those in eqs A15−A17, we obtain the following implicit expression of θ as a function of the bulk surfactant concentration c (cf. eq 38 of ref 50, with $\bar{\imath} = M_0 = 0$):

$$1 - \theta\exp(a\theta)/[\beta c(1-\theta-S)] = \xi\theta \quad \text{(A20)}$$

where ξ retains the same significance as in eq A17. The numerical values of θ as functions of c can be readily obtained from the implicit expression of eq A20 by some iterative procedure, e.g. by the Newton−Raphson method. Differentiating θ in eq A20 with respect to t yields the following expression of θ':

$$\theta' = \frac{\xi\psi\theta(1-\theta-S)^2/(2t) - S'\theta\exp(a\theta)}{\xi\psi(1-\theta-S)^2 + [1-S+a\theta(1-\theta-S)]\exp(a\theta)} \quad \text{(A21)}$$

which is solved together with the differential equations (A9) and (A13) by the fourth-order Runge−Kutta method.

Case 3. Progressive Polynucleation with Decay of the Nucleation Centers. An approximate account for the exponential decay of the nucleation centers requires exclusively a modification of the expression for S''_x in eq A13. Upon assuming as a first approximation that θ varies with time slowly enough as to permit us to bring θ^n outside the integral sign in eq A5, we obtain

$$\frac{dN}{dt} \cong N_0k_N\theta^n\exp(-k_N\theta^n t) \quad \text{(A22)}$$

Substitution of this approximate expression into the general equation (A12) yields

$$S''_x = K\sqrt{S'_x}\theta^{(n/2+1)}e^{-k_N\theta^n t/2} + S'_x[n\theta'/\theta - k_N(n\theta^{n-1}\theta' t + \theta^n)] \quad \text{(A23)}$$

where K is still defined by eq A14.

Cases 1 and 2 can account approximately for polynucleation with decay of the nucleation centers by merely replacing eq A13 by eq A23, while leaving unaltered all other expressions required for the solution of the pertinent case.

Case 4. The Ingestion Effect. Even the ingestion effect can be included in cases 1 and 2 by merely modifying the differential equation for S''_x. Substitution of the nucleation rate of eq A7, which accounts for this effect, into the general expression of eq A12 yields

$$S''_x = K\sqrt{(1-S)S'_x}\theta^{(n/2+1)} + S'_x[n\theta'/\theta - S'/(1-S)] \quad \text{(A24)}$$

which replaces eq A13.

Appendix II

Since eq 5 holds during the whole process up to the attainment of the steady-state differential capacity, the Avrami equation

will be written as usual:

$$dS_{II}/dt = (1 - S_{II})\, dS_{II,x}/dt \qquad (A25)$$

By considerations analogous to those leading to eq A8, the rate of radial growth of the clusters of phase II following the I → II transition is given by

$$dR_{II}/dt = v_{II,R} = k_{II,R}S_I = k_{II,R}(1 - S_{II}) \qquad (A26)$$

Following Avrami,[29,48] the relationship between S_w and the corresponding "extended area" $S_{w,x}$ will be obtained by considering that the rate of increase of the area covered by aggregates is an extensive property of the system and, as such, must be regarded as proportional to the "available area". If, *ab absurdo*, each water aggregate were in a condition of growing without the limitations imposed by the other aggregates, the available area per unit surface would be equal to S_{II}, and hence the rate of increase of the hypothetical extended area will be given by $dS_{w,x}/dt = kS_{II}$, where k is a proportionality constant. As a matter of fact, the actual area available for the growing water clusters is that, $S_{II} - S_w$, still uncovered, whence $dS_w/dt = k(S_{II} - S_w)$. Upon eliminating the common value of k between the two relationships we obtain

$$dS_w/dt = (1 - S_w/S_{II})\, dS_{w,x}/dt \qquad (A27)$$

The random adsorption of uracil molecules into the water aggregates obeys the following Frumkin isotherm:

$$\beta c = \frac{\theta}{S_w - \theta} \exp(a\theta) \qquad (A28)$$

with the same β and a values as in eq A19. The difference between this equation and eq A19 is due to the fact that the maximum possible value attained by θ is now S_w. Moreover, the volume concentration $\bar{c}$ at the electrode surface in eq A19 is now replaced by the corresponding bulk concentration c since, at the bulk concentrations adopted in our measurements and in the time scale of the C vs t curves, any depletion of the surfactant molecules in the proximity of the electrode surface is replenished almost instantaneously.

Substitution of $v_{II,R}$ and $v_{II,N}$ from eq A26 and 6 into the general equation (A12) yields

$$S''_{II,x} = K_{II}(1 - S_{II})\sqrt{S'_{II,x}} \quad \text{with} \quad K_{II} \equiv 2v_{II,R}(gv_{II,N})^{1/2} \qquad (A29)$$

Analogously, by substituting $v_{w,N}$ and $v_{w,R}$ from eqs 7 and 8 into eq A12, we obtain

$$S''_{w,x} = K_w[1 - (1 + \zeta)\theta]\sqrt{S'_{w,x}} \quad \text{with}$$

$$K_w \equiv 2k_e(gv_{w,N})^{1/2}; \quad \zeta = \frac{k_c}{k_e} \qquad (A30)$$

The set of the four differential equations (A25), (A27), (A29), and (A30) is solved by the fourth-order Runge−Kutta method; the surface coverage θ in eq A30 is calculated as a function of c via the implicit equation (A28) by using the Newton−Raphson iterative procedure.

References and Notes

(1) Buess-Herman C. In *Adsorption of Molecules at Metal Electrodes*; Lipkowski, J., Ross, P. N., Eds.; VCH: New York, 1992; pp 77−118.
(2) De Levie, R. *Chem. Rev.* **1988**, *88*, 599−609.
(3) Batrakov, V. V.; Damaskin, B. B.; Ipatov, U. P. *Elektrokhimiya* **1974**, *10*, 144−147.
(4) Stolberg, L.; Lipkowski, J.; Irish, D. E. *J. Electroanal. Chem.* **1987**, *238*, 333−353.
(5) Stolberg, L.; Morin, S.; Richer, J.; Lipkowski, J. *J. Electroanal. Chem.* **1991**, *307*, 241−262.
(6) Hamelin, A.; Morin, S.; Richer, J.; Lipkowski, J. *J. Electroanal. Chem.* **1991**, *304*, 195−209.
(7) Popov, A.; Naneva, R.; Dimitrov, N.; Vitanov, T.; Bostanov, V.; de Levie, R. *Electrochim. Acta* **1992**, *37*, 2369−2371.
(8) Hölzle, M. H.; Kolb, D. M. *Ber. Bunsen-Ges. Phys. Chem.* **1994**, *98*, 330−335.
(9) Scharfe, M.; Hamelin, A.; Buess-Herman, C. *Electrochim. Acta* **1995**, *40*, 61−67.
(10) Buess-Herman, C. *Prog. Surf. Sci.* **1994**, *46*, 335−375.
(11) Hölzle, M. H.; Wandlowski, Th.; Kolb, D. M. *Surf. Sci.* **1995**, *335*, 281−290.
(12) Wandlowski, Th. *J. Electroanal. Chem.* **1995**, *395*, 83−89.
(13) Hölzle, M. H.; Krznaric, D.; Kolb, D. M. *J. Electroanal. Chem.* **1995**, *386*, 235−239.
(14) Wandlowski, Th.; Lampner, D.; Lindsday, S. M. *J. Electroanal. Chem.* **1996**, *404*, 215−226.
(15) Tao, N. J.; de Rose, J. A.; Lindsday, S. M. *J. Phys. Chem.* **1993**, *97*, 910−919.
(16) Wandlowski, Th. *J. Electroanal. Chem.* **1990**, *293*, 219−236.
(17) Wandlowski, Th.; Pospísil, L. *J. Electroanal. Chem.* **1989**, *258*, 179−192.
(18) Wandlowski, Th.; Pospísil, L. *J. Electroanal. Chem*. **1989**, *270*, 319−329.
(19) Canac, F. *Hebd. C. R. Seances Acad. Sci.* **1933**, *196*, 51−63.
(20) Kolmogorov, *A. N. Bull. Acad. Sci. USSR/Sci. Math. Nat.* **1937**, *3*, 355−371.
(21) Avrami, M. *J. Chem. Phys.* **1939**, *7*, 1103−1112.
(22) Evans, U. R. *Trans. Faraday Soc.* **1945**, *41*, 365−374.
(23) Pospísil, L. *J. Electroanal. Chem.* **1986**, *206*, 269−283.
(24) Pospísil, L.; Hanzlík, J.; Fuoco, R.; Fanelli, N. *J. Electroanal. Chem.* **1992**, *334*, 309−321.
(25) Hölzle, M. H.; Retter, U.; Kolb, D. M. *J. Electroanal. Chem.* **1994**, *371*, 101−109.
(26) Noel, M.; Chandrasekaran, S.; Ahmed Basha, C. *J. Electroanal. Chem.* **1987**, *225*, 93−109.
(27) Bosco, E.; Rangarajan, S. K. *J. Chem. Soc., Faraday Trans. 1* **1981**, *77*, 1673−1696.
(28) Bhattacharjee, B.; Rangarajan, S. K. *J. Electroanal. Chem.* **1991**, *302*, 207−218.
(29) de Levie, R. In *Advances in Electrochemistry and Electrochemical Engineering;* Gerischer, H., Tobias, C. W., Eds.; Wiley: New York, 1985; Vol. 13, pp 1−67.
(30) Wandlowski Th.; de Levie R. *J. Electroanal. Chem.* **1993**, *352*, 279−294.
(31) Foresti, M. L.; Innocenti, M.; Hamelin, A. *Langmuir* **1995**, *11*, 498−505.
(32) Foresti, M. L.; Innocenti, M.; Guidelli, R. *J. Electroanal. Chem.* **1994**, *376*, 85−95.
(33) Aloisi, G., Cavallini, M., Bracali, M. Unpublished results.
(34) Magnussen, O. M.; Ocko, B. M.; Wang, J. X.; Adzic, R. R. *J. Phys. Chem.* **1996**, *100*, 5500−5508.
(35) Magnussen, O. M.; Ocko, B. M.; Adzik, R. R.; Wang, J. X. *Phys. Rev. B: Condens. Matter* **1995**, *51*, 5510−5513.
(36) Ocko, B. M.; Magnussen, O. M.; Wang, J. X.; Wandlowski, Th. *Phys. Rev. B: Condens. Matter* **1996**, *53*, R7654-R7657.
(37) Wandlowski, Th.; Wang, J. X.; Magnussen, O. M.; Ocko, B. M. *J. Phys. Chem.* **1996**, *100*, 10277−10287.
(38) Foresti, M. L.; Aloisi, G.; Innocenti, M.; Kobayashi, H.; Guidelli, R. *Surf. Sci.* **1995**, *335*, 241−251.
(39) de Levie, R.; Wandlowski, Th. *J. Electroanal. Chem.* **1994**, *366*, 265−270.
(40) Gierst, L.; Franck, C.; Quarin, G.; Buess-Herman, Cl. *J. Electroanal. Chem.* **1981**, *129*, 353−363.
(41) Bosco, E.; Rangarajan, S. K. *J. Chem. Soc., Faraday Trans. 1* **1981**, *77*, 483−495.
(42) Angerstein-Kozlowska, H.; Conway, B. E.; Klinger, J. *J. Electroanal. Chem.* **1978**, *87*, 301−320.
(43) Nürnberg, H. W.; Wolff, G. *Collect. Czech. Chem. Commun.* **1965**, *30*, 3785−3793.
(44) Kim, M. H.; Christian, S. D.; Dryhurst, G. *J. Electroanal. Chem.* **1979**, *104*, 165−183.
(45) Valette, G. *J. Electroanal. Chem.* **1989**, *269*, 191−203.
(46) Guidelli, R.; Foresti, M. L. *J. Electroanal Chem.* **1986**, *197*, 103−121.
(47) Guidelli, R.; Aloisi, G. *J. Electroanal. Chem.* **1994**, *373*, 107−114.
(48) Avrami, M. *J. Phys. Chem.* **1940**, *8*, 212−224.
(49) Guidelli, R. *J. Electroanal. Chem.* **1971**, *33*, 291−303.
(50) Guidelli, R.; Pezzatini, G. *J. Electroanal. Chem.* **1977**, *84*, 211−234.

JP961663Z